

OBSERVATION OF CONTINUOUS MODE CONVERSION OF LAMB WAVES IN COMPOSITE PLATES FOR SHM

Bianca Hennings*, **Rolf Lammering†**

Helmut-Schmidt-University/ University of the Federal Armed Forces Hamburg
Holstenhofweg 85, D-22043 Hamburg

*bianca.hennings@hsu-hh.de

†rolf.lammering@hsu-hh.de

Keywords: fiber composites, material modeling, structural health monitoring, LAMB-waves, quasi-continuous mode conversion.

Summary: *This work presents mode conversion effects in carbon fiber reinforced plastic plates. The optically observed pattern of wave propagation, which include the inhomogeneity of the material and additionally the information of eventually existing defects will be discussed. Furthermore, the modeling of the carbon fiber reinforced plastic for subsequent finite element analysis of wave propagation in plates from this material will be presented. The random distribution of fibers in the matrix material has to be considered in a microscale model to properly capture the “quasi-continuous mode conversion”. Finally, a numerical example will show the influence of the material model on the developing wave modes.*

1. INTRODUCTION

Modern infrastructure includes a vast variety of structural systems which have to be kept under surveillance in order to avoid malfunction and accidents. Typical examples are steel and concrete bridges, pressure vessels, railway tracks, and transmission lines, to name just a few. Especially aerospace structures are in the focus of improved inspection techniques since a considerably amount of life cycle costs is due to inspection and repair and since damage can lead to catastrophic failure. A reliable monitoring technique would allow for adjusted maintenance intervals in accordance to the real requirements so that a reduction of the operating costs can be expected.

Because of the reasons above mentioned, current research on structural health monitoring methods and non-destructive testing techniques aims at fast, efficient, and reliable detection of visible and hidden structural damages in engineering structures.

The difficulty in identifying the damage is often caused by the complex phenomena of damage initiation and evolution including various failure modes which have to be detected reliably. Among others, techniques based on elastic waves play an important role for damage detection. In plate and shell structures, especially high frequency waves, i.e. guided waves or LAMB-waves, cf. GRAFF [4], and their possible contributions to structural health monitoring methods

are in the focus of current research, cf. GIURGIUTIU [3]. Reflections, refractions or mode conversions are distinct indications of faults or defects and are often instantaneous visible in the pattern of an otherwise undisturbed propagating wave.

Beyond that, the increasing application of fiber reinforced plastics in lightweight structures is currently demanding for advanced monitoring techniques. Thus LAMB-wave based techniques are investigated for potential use in carbon fiber reinforced plastic structures. However, with the anisotropic behavior of this class of materials and their layered structure in mind, the arising physical phenomena are more complicated and the interpretation of the observed LAMB-wave behavior becomes more challenging, cf. ROSE [8].

This work deals with the observation of a phenomenon which is called “quasi-continuous mode conversion”, cf. NEUMANN ET AL. [7] and WILLBERG ET AL. [9]. It appears after the fastest guided wave (S_0 -wave in isotropic solids) has passed the observed area and before the second-fastest wave (A_0 -wave in isotropic solids) arrives. In this time period, regular patterns occur which are not seen in isotropic solids. This phenomenon is observed in thin-walled fiber reinforced plastic material with arbitrary fiber orientation and lay-up or with woven fabrics.

The manuscript is structured as follows: First, the experimentally observed quasi-continuous mode conversion is described in detail. In a next step, possible reasons of the quasi-continuous mode conversion are discussed and the material inhomogeneity is identified as the source. Then, a stochastic inhomogeneity is implemented into the material law, cf. HENNINGS [5]. Subsequently, numerical investigations show that this phenomenon can be captured in this way.

2. THEORETICAL FOUNDATIONS

2.1 Waves in elastic plates

In the analysis of wave motion in elastic media the balance of momentum ($\boldsymbol{\sigma}$: stress tensor, ρ : material density, \mathbf{b} : distributed volume specific body forces, \mathbf{u} : displacement field, superposed dot: differentiation with respect to time)

$$\operatorname{div} \boldsymbol{\sigma} + \rho \mathbf{b} = \rho \ddot{\mathbf{u}}, \quad (1)$$

the linear strain-displacement relation (linear GREEN-LAGRANGIAN strain tensor \mathbf{E})

$$\mathbf{E} = \frac{1}{2}(\operatorname{grad} \mathbf{u} + \operatorname{grad}^T \mathbf{u}), \quad (2)$$

as well as HOOKE’s law (fourth order elasticity tensor \mathbb{C})

$$\boldsymbol{\sigma} = \mathbb{C} : \mathbf{E} \quad (3)$$

are combined to obtain

$$\operatorname{div}(\mathbb{C} : \operatorname{grad} \mathbf{u}) + \rho \mathbf{b} = \rho \ddot{\mathbf{u}}. \quad (4)$$

In the case of isotropic material HOOKE’s law can be expressed by the LAMÉ-constants λ and μ and Eq. (4) may be rewritten as

$$(\lambda + \mu) \operatorname{grad}(\operatorname{div} \mathbf{u}) + \mu \operatorname{div}(\operatorname{grad} \mathbf{u}) = \rho \ddot{\mathbf{u}} \quad (5)$$

which is well-known as LAMÉ-NAVIER differential equation. Solutions of the differential equation (5) are given in many textbooks, cf. ACHENBACH [1] or GRAFF [4], and are not repeated here for brevities sake.

In an unbounded elastic media it is well known that two and only two types of waves are propagated, namely the compression (P-) wave and the shear (S-) wave. These types of waves are fundamental to the following considerations.

In the case of semi-infinite media the existence of a boundary comes into play and distinguishes this problem from the latter. The analysis leads to the phenomenon of mode conversion that occurs when waves encounter a free boundary. This means that in the case of an incident P- or S-wave, both a P-wave as well as an S-wave may be reflected. Similar effects are observed at the interface between two elastic layers. In the analysis of the reflections SNELL's law is fundamental. The result of the respective mathematical problem, i.e. differential equations including boundary condition is interpreted as a surface wave which is a third type of wave. These waves have been named after LORD RAYLEIGH who showed that their amplitudes decrease rapidly with depth. Depending on POISSON's ratio of the media the velocity of propagation is somewhat less than shear velocity. RAYLEIGH waves are non-dispersive.

LAMB-waves belong to another type of waves which is found in traction-free thin plate and shell structures. Their formation may be considered as a consequence of P- and S-wave reflections at the surfaces of plates and shells. Many textbooks, e.g. GRAFF [4], deal with the LAMB-wave theory for isotropic media which is not repeated here for that reason. From the analytical solution of the governing equations one obtains finally the RAYLEIGH-LAMB-equation

$$\frac{\tan qd}{\tan pd} = - \left[\frac{4k^2 pq}{(q^2 - k^2)} \right]^{\pm 1} . \quad (6)$$

The parameters p and q are defined as $p^2 = \omega^2/c_L^2 - k^2$ and $q^2 = \omega^2/c_T^2 - k^2$. Furthermore, k stands for the wave number, ω for the excitation frequency, and c_L and c_T for the phase velocities of the longitudinal and transversal waves, respectively. The numerical solution of Eq. (6) with the exponent +1 yields the symmetric eigenvalues, with consideration of the exponent -1 the antisymmetric eigenvalues. The results show that an infinite number of wave modes propagates in plates and that at least two modes exist at any frequency. In structural health monitoring the fundamental symmetric (S_0) and antisymmetric (A_0) modes are typically generated without excitation of higher modes. LAMB-waves are generally dispersive. They are able to propagate over long distances in thin plate and shell structures with low attenuation so that they are attractive for health monitoring techniques. Due to their short wavelength LAMB-waves are also applicable for the detection of small faults.

In the case of transversal isotropic media, e.g. a single layer of carbon fiber reinforced plastic material, the derivation of the result corresponding to Eq. (6) is much more sophisticated, cf. HENNINGS [5] or ROSE [8], and is not presented here for brevities sake. Instead of the analytical expressions the graphical visualization is shown in Figs. 1 and 2 as dispersion diagrams for fiber orientations of 0° and 45° , respectively.

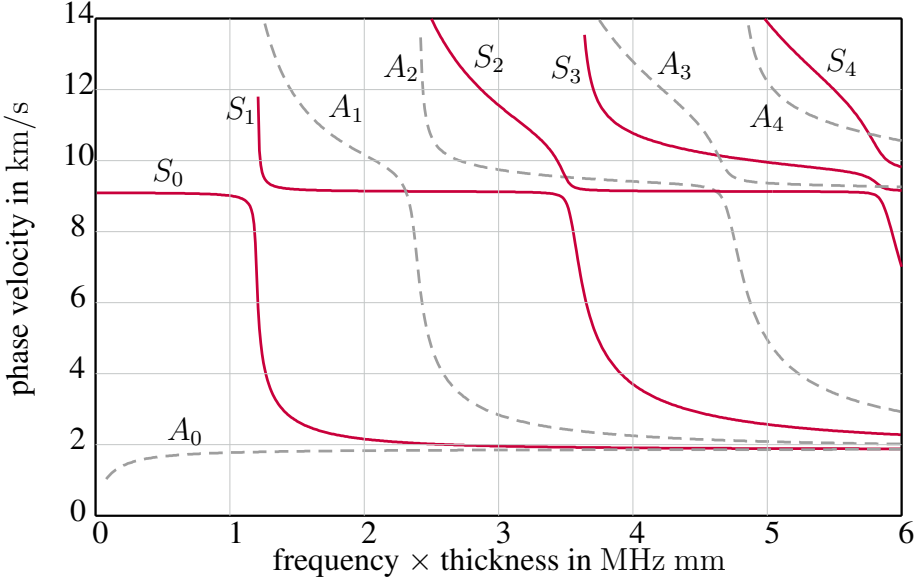


Figure 1: Dispersion diagram of a single unidirectional layer in fiber orientation (0°-layer)

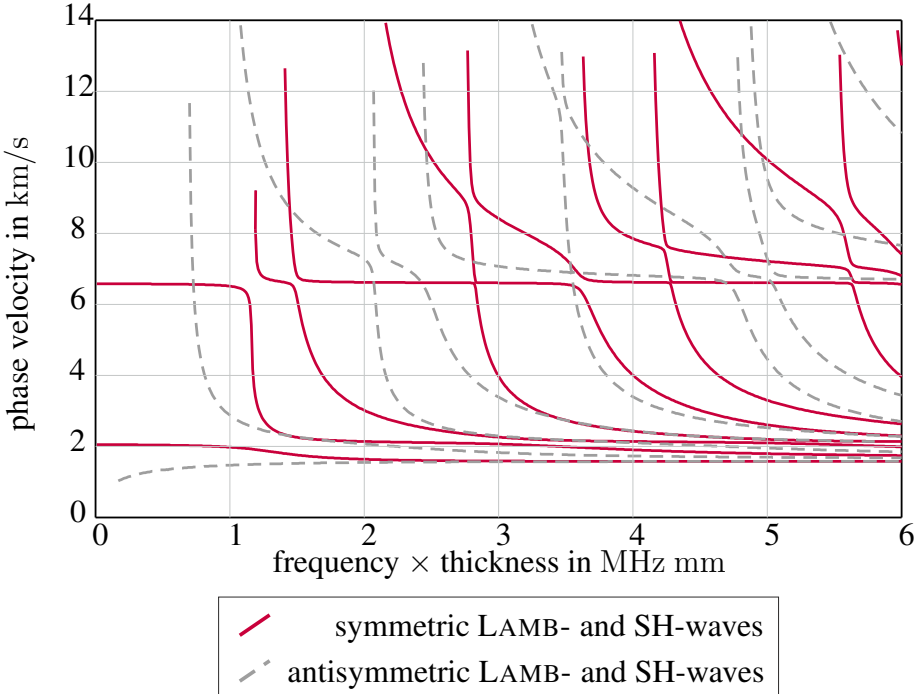


Figure 2: Dispersion diagram of a single unidirectional layer in fiber orientation (45°-layer)

It becomes visible, that the dispersion diagram for wave propagation in fiber direction, cf. Fig. 1, is quite similar to the isotropic case. Here, the symmetric (S_i) and antisymmetric (A_i) modes can clearly be distinguished. This is not the case for wave propagation at the angle of 45° with respect to the fiber orientation. Therefore, the various curves are not marked in Fig. 2. Furthermore, SH-waves (shear horizontal waves) are included in Fig. 2.

2.2 Material modeling

Carbon fiber reinforced plastic material is composed from the carbon fiber and the shaping matrix material as depicted in Fig. 3, where a lay-up with four layers in an orientation of $[0^\circ, 90^\circ]_s$ is shown. The physical structure (left picture) is transferred to a fiber-matrix-model on the micro-scale. Here, both components are described by their individual material properties (center picture). Now, an appropriate homogenization technique, e.g. the semi-empirical homogenization method of HALPIN & TSAI, cf. JONES [6], is applied in order to obtain the fiber-matrix model on the macro-scale (right picture). This procedure leads to a layer-wise homogeneous structure. In a subsequent re-consideration, this idealization will be reviewed and an enhanced material model will be proposed.

3. QUASI-CONTINUOUS MODE CONVERSION (QCMC)

To clearly explain the phenomenon of “quasi-continuous mode conversion”, the difference of LAMB-wave propagation in carbon fiber reinforced plastic (CFRP) plates compared to that in an isotropic one is pointed out.

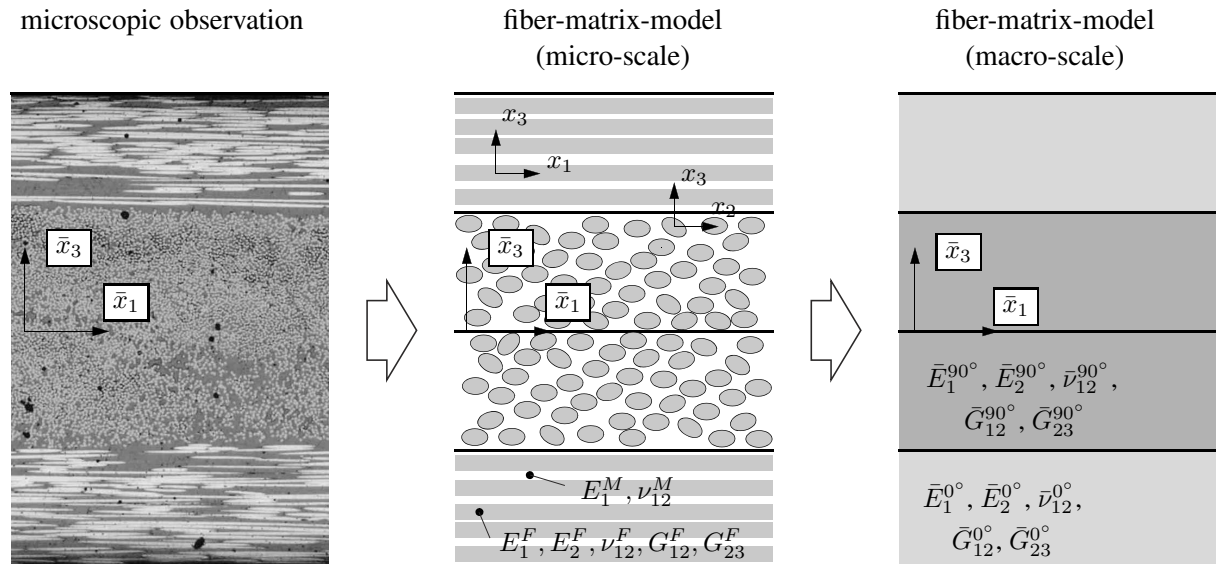


Figure 3: Material modeling: from microscopy to fiber-matrix-model

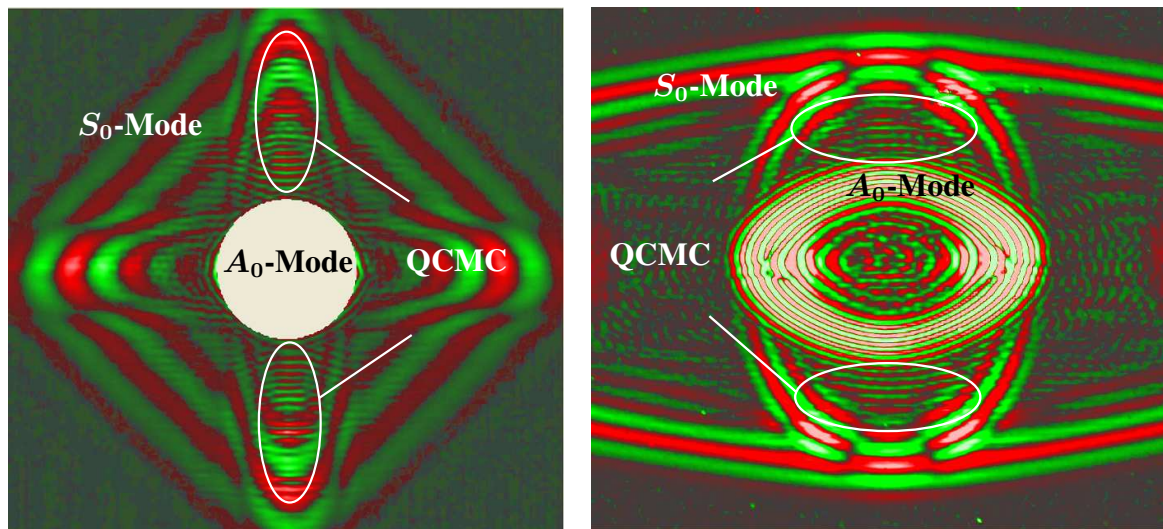
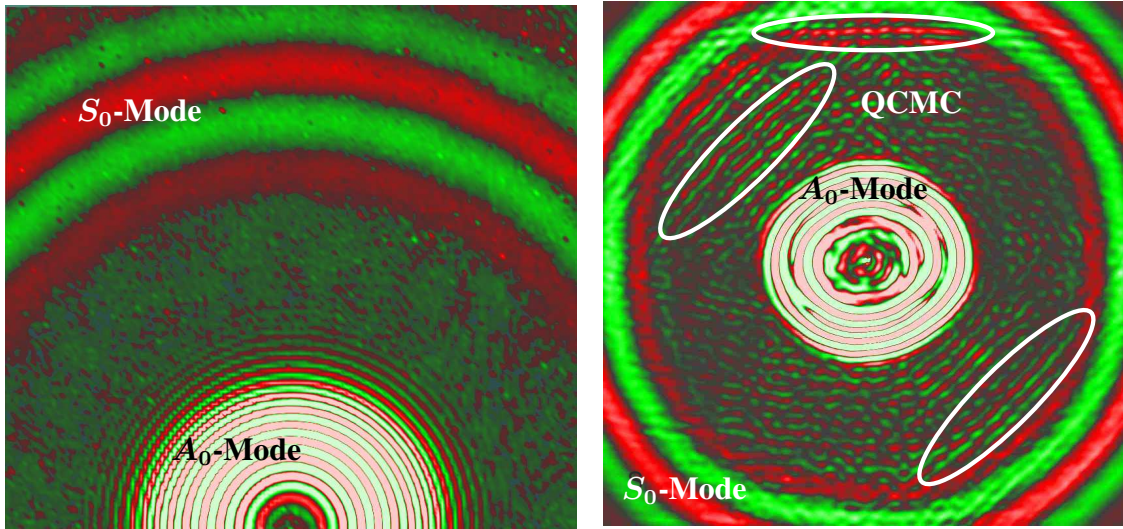


Figure 4: Measured wave propagation via scanning laser vibrometry

Figure 4a shows the experimental investigation of the fundamental S_0 - and A_0 -modes in an intact aluminium plate (thickness: 1 mm) taken with a scanning laser vibrometer. As expected, the transiently excited primarily S_0 - and A_0 -wave groups propagating with their inherent phase velocity and wave length and separating in a certain travelling time without any mode conversion. As mentioned before, an almost identical behavior is expected from transiently excited wave groups in intact CFRP laminates.

However, recent experimental investigations showed irregularities from this regular pattern in assumedly undamaged CFRP plates, which can be seen in the following examples. The wave propagation in a quasi-isotropic plate exclusively composed of unidirectional (UD) layers [UD255 0°/ UD500 \pm 45°/ UD255 90°]_S is shown in Figure 4b. The faster S_0 - and slower A_0 -waves occur and move as expected, but the arising waves between the primary excited symmetric and antisymmetric wave groups, highlighted by white ellipses, represent an anomaly in the wave behavior. Wave length and propagation velocity of these “new” waves point toward additional A_0 -waves. Though, these secondary A_0 -waves appear farther from the excitation point than the primary excited ones.

Beside quasi-isotropic laminates, this phenomenon is also observed in cross-pplies as well as in UD laminates, (cf. Fig. 4c, 4d). Since the secondary A_0 -waves immediately appear in the whole plate during and after passing of the S_0 -wave field, this behavior implies “quasi-continuous” mode conversion. In all of the investigated laminates, the secondary A_0 -wave fronts run almost parallel to the fiber direction of the near surface layers. Furthermore, animated measurements identify them as secondary A_0 -waves propagating in same and opposite direction of the primary excited wave groups, as well as standing waves.

4. ENHANCED MATERIAL MODELING

In numerical computations the described wave phenomenon cannot be represented by the conventionally utilized complete homogenization of the single layers in a laminate. Therefore, an enhanced material modeling approach, which enables the realistic reproduction of the QCMC effect, is presented in this section.

Figure 5 shows the details of two photomicrographs of a single UD-layer with fibers in x_1 -direction. In both sectional views it can be seen that the assumption of uniformly distributed fibers does not reflect the reality. On closer inspection, obviously, the global fiber volume ratio φ_f of a single layer does not correspond to the local fiber-matrix ratio. This fact is clearly evident in Figure 5b, where the randomly distributed fibers may form regions with a considerably lower fiber volume ratio, e.g. in the upper left corner.

Since the QCMC phenomenon does not just occur in complex anisotropic laminates but already in the simplest case of a single layer UD-plate this particular type of plate is considered for development of enhanced material modeling. For the simulation of wave propagation the three-dimensional problem (plate with actuator at the top and/or bottom surfaces) is reduced to a two-dimensional plane strain plate, cf. Fig. 6 (top) and Fig. 7. Additionally, the boundary conditions are introduced in the axis of symmetry and the excitation of the actuators is replaced by nodal forces. They act in the same or in opposite direction dependant on whether symmetric

or antisymmetric waves are to be generated.

A look at the 90° -sectional view of the UD layer motivates a novel approach with sectorized homogenized zones. Figure 6 shows the procedure to generate the enhanced model by means of a single UD layer with a thickness of 0.4 mm.

In a first step the fiber-matrix-model is viewed on the micro scale. The fibers are idealized depicted as squares (black) with an edge length ($8\ \mu\text{m}$) corresponding to the dimension of a real fiber diameter ($5 - 10\ \mu\text{m}$). Furthermore, the fibers are randomly distributed (GAUSSIAN distribution) in the matrix material (represented by white squares) in consideration of the global fiber volume ratio. Here, each square corresponds to a single finite element. The resulting high-resolution numerical model is able to reproduce the QCMC effect. However, due to the vast number of degrees of freedom (DOF) this model is unsuitable for efficient numerical evaluation.

In the next step the micro-model will be divided into subsets. Both center pictures in Figure 6 show the same detail of the micro-model with their respectively subsets, which are composed of an arbitrary square number of fiber-matrix-elements and are highlighted by colored frames. Since the primary allocation of fiber and matrix elements is randomly distributed, the fiber volume ratio of every subset can differ from the global ratio.

Subsequently, the material properties (YOUNG's modulus, POISSON ratio, shear modulus) of each subset are determined by using the semi-empirical homogenization method of HALPIN & TSAI, cf. JONES [6]. With displacement amplitudes and wave velocity in mind, this method offers the best approximation to the values of the micro-model. Due to the fact that now all elements in a subset have the same material parameters, the sectorized homogenization allows a coarser discretization as the micro-model, so that every subset in the meso-model can be expressed by only one finite element. The shades of gray in the bottom pictures of Figure 6 correlate to the local fiber volume ratio of the subsets, in which brighter squares reflect a higher matrix concentration than darker ones.

The subsets of the left meso-model show marginal variations in coloring resp. fiber volume ratio, whereas the color changes (and with this the different fiber volume ratios) are clearly

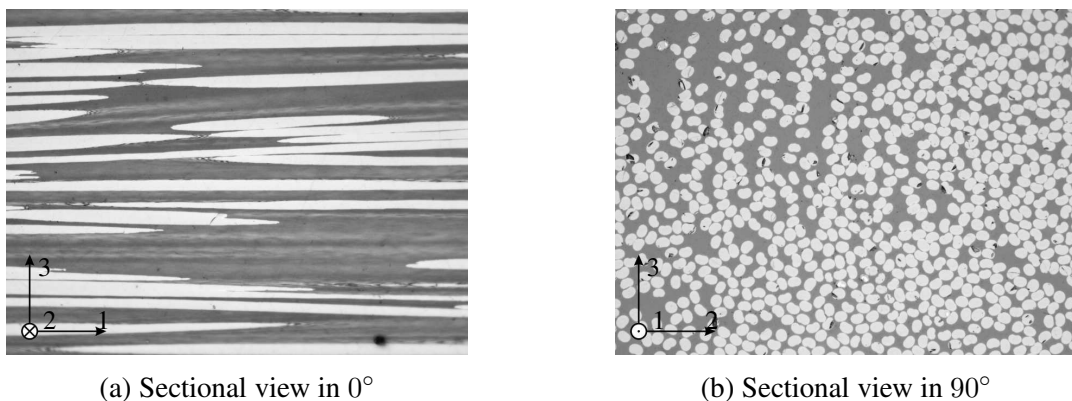


Figure 5: Detail of photomicrographs of a single UD-layer (fibers in x_1 -direction)

visible in the right meso-model. The reason for this is the number of fiber and matrix elements per subset. The smaller the number of elements, the stronger is the influence of the random distribution of fiber and matrix, which arises in the deviation from the global fiber volume ratio.

5. RESULTS

The dimensions of the micro-model of a single UD layer (fibers in x_2 -direction) are illustrated in Figure 7. The material parameters of fibers and matrix material are listed in Table 1. The fiber volume ratio is $\varphi_f = 0.5$. Based on the edge length of $8 \mu\text{m}$ the micro-model consists of 12500×50 squared fiber-matrix-elements (FM elements).

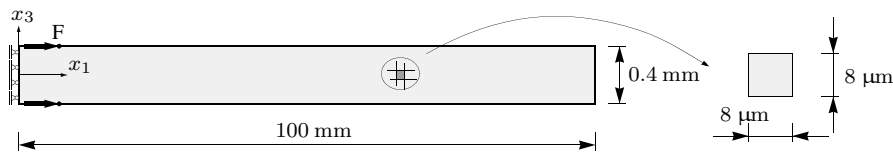


Figure 7: Dimensions of the micro-model and a fiber-matrix-element (FM element).

Originating from the micro-model different meso-models are created, in which various squared numbers of FM elements ($2 \times 2/ 5 \times 5/ 10 \times 10/ 25 \times 25/ 50 \times 50$ elements) are combined to subsets, cf. Figure 8. As mentioned in the section before, each subset is discretized by one finite element with its homogenized material properties. The computation of wave propagation in this meso-models is supposed to answer the question at which homogenization level of the layer the QCMC effect can be reproduced.

Table 2 shows the information of the micro and meso-models concerning element distribution and local fiber volume ratios. The first rows lists the number of subsets of each model. Every subset is represented by a 9-node element (2 DOF per node) and thus leads to the total number of DOF for each model shown in the second row.

Due to the mergence of fiber and matrix elements there are different fiber volume ratios φ_f^e in the subsets. The number of occurring ratios as well as their minimum and maximum are listed in line 3 to 5. It is evident that the number of local fiber volume ratios rises with an increasing number of FM elements per subset (see Tab. 2 line 3). Simultaneously, the minimum and maximum values converge to the global fiber volume ratio of the layer ($\varphi_f = 0.5$).

The excitation of the plate takes place at 2.5 mm from the left edge (symmetry axis) at a load

Table 1: Material properties of fiber and matrix

Material	$E_{ }$ [GPa]	E_{\perp} [GPa]	ν_{\perp} [-]	$\nu_{\perp\perp}$ [-]	G_{\perp} [GPa]	ρ [kg/m ³]
Fiber	200	16.7	0.2	0.2	83	1800
Matrix	3.5	-	0.4	-	-	1400

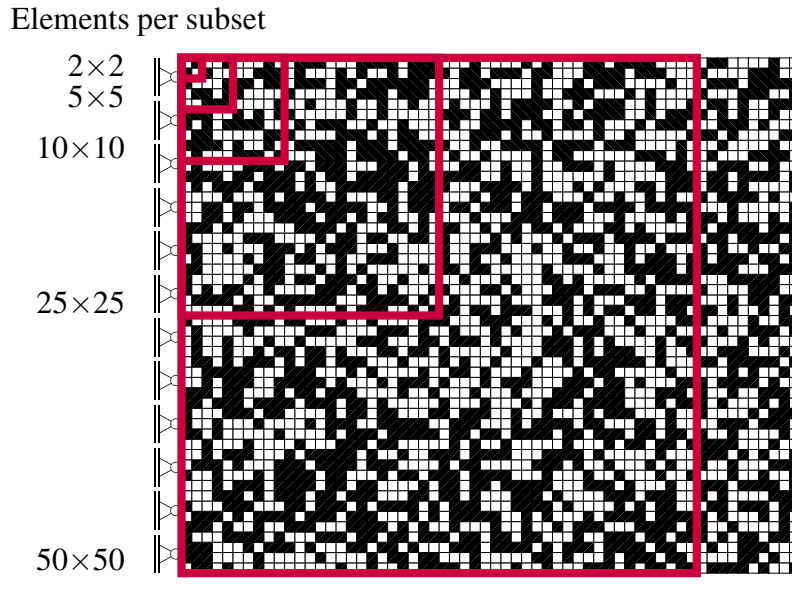


Figure 8: Detail of the micro-model with illustration (red squares) of the subsets

of 100 N applied as a two cycle sine burst signal with a central frequency of 100 kHz. Over two cycles the sine signal is multiplied by a HANNING window. Since the effect of QCMC occurs after the symmetric waves are passing the plate the structure is excited symmetrically.

Figure 9 shows the results of the numerical simulation. The red curves display the out-of-plane displacements (u_3) of the different meso-models at the top edge of the plate. For comparison also the displacement amplitudes of the micro-model calculation (black curves) are depicted in the diagrams.

At the time of $t = 49.5 \mu\text{s}$ the primary excited S_0 -wave has passed the whole plate and reached the right end of the structure. As expected, due to the random allocation of FM elements

Table 2: Model parameter

FM elements/subset	meso-models					micro-model
	2×2	5×5	10×10	25×25	50×50	(1×1)
Subsets	156 250	25 000	6 250	1 000	250	(625 000)
DOF	1 275 051	210 021	55 011	10 005	3 003	5 050 101
Number of φ_f^e	5	18	37	73	95	2
$\min(\varphi_f^e)$	0	0.16	0.29	0.437	0.464	0
$\max(\varphi_f^e)$	1	0.84	0.68	0.563	0.532	1

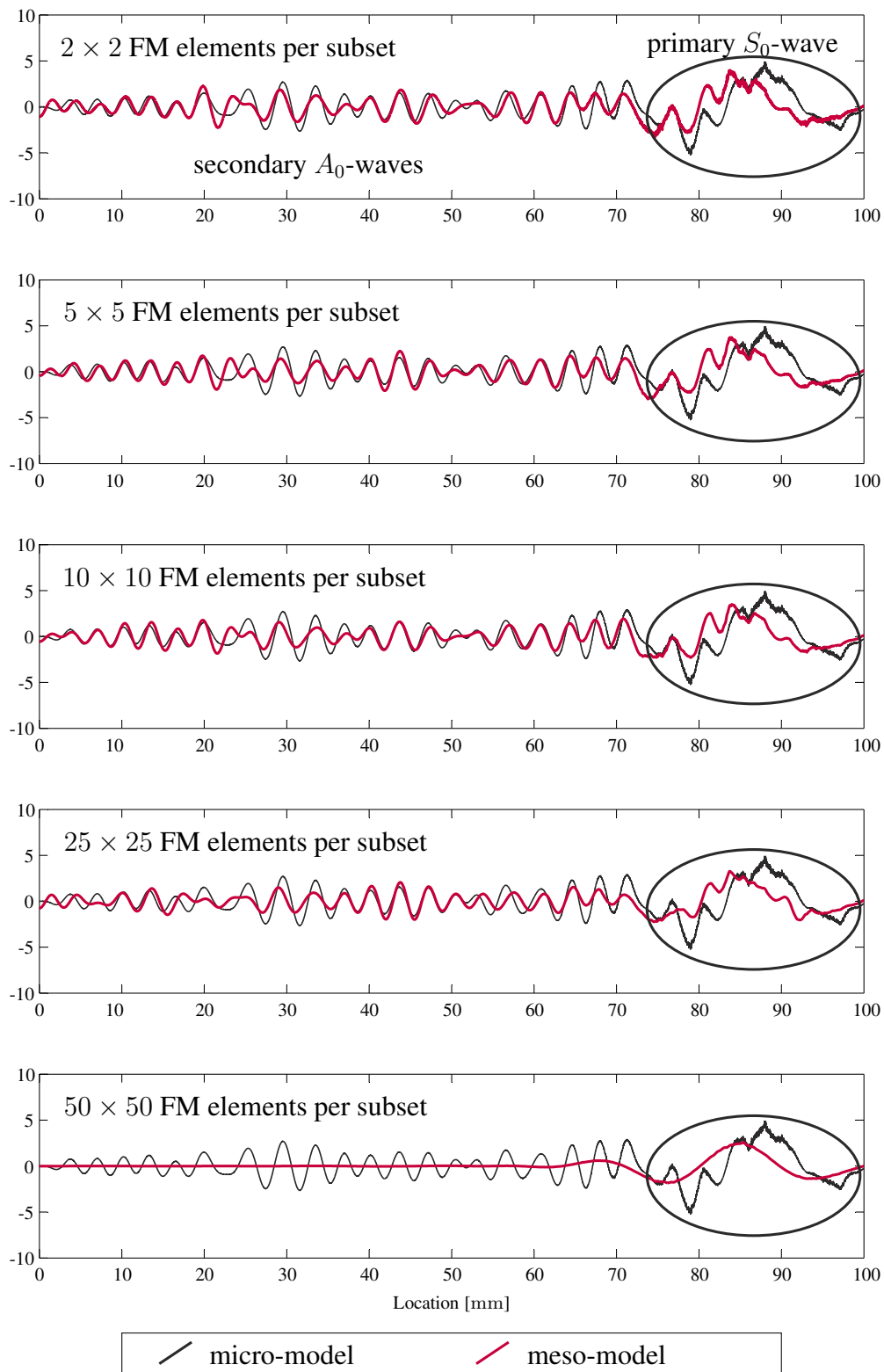


Figure 9: Out-of-plane-displacements [nm] of the UD plate at the top edge by using variously sized subsets ($t = 49.5 \mu\text{s}$).

the displacement curves of the micro-model show secondary A_0 -wave groups appearing after the symmetric waves have passed the plate. These secondary wave groups are propagating in same and opposite direction of the primary excited S_0 -wave and moreover they appear locally as standing waves.

As it can be seen in Figure 9, every meso-model is able to reproduce this behavior, except the model with the coarsest discretization (50×50 FM elements per subset). Even the meso-model with 25×25 FM elements per subset is able to capture the amplitudes of the secondary A_0 -wave in an excellent manner and shows the peaks of the primary excited S_0 -wave. The offset of the S_0 -displacement curves between the micro and meso-model is owed to the homogenization method and is not a consequence of the application of subsets.

The reason for the absence of secondary A_0 -waves in the coarsest meso-model with 50×50 FM elements per subset is not explained by a bad discretization resp. oversized finite elements. Also these finite elements (length of 0.4 mm) are 10 times smaller than the A_0 -waves (wave length $\lambda_a \approx 4$ mm). Since this meso-model uses only one finite element across the thickness, the structure gets a symmetric set-up relating to the midplane of the plate and for this reason no conversion from S_0 - to A_0 -mode happens, see AHMAD [2].

6. CONCLUSION

An enhanced material modeling method for single UD layer is presented. Here, compared to the conventional layer-wise homogenization, size-varying subsets with homogenized material properties are generated to successfully reproduce the phenomenon of “quasi-continuous mode conversion” in this particular type of CFRP plates. For the homogenization the semi-empirical method of HALPIN& TSAI is applied.

Investigations concerning the maximum size of the subregions for simulating the “quasi-continuous mode conversion” yield at least two subregions over the height of the UD layer, but solely to ensure an asymmetric set-up of the numerical model because of the varying material parameters of the subsets. Additionally taking into account the common restrictions as node number resp. polynomial degree per expected wave length the enhanced material model excellently simulates the real propagation behavior in UD layers and thus motivates the need for a stochastic material model for proper analysis of wave propagation.

References

- [1] J. Achenbach, *Wave propagation in elastic solids*. Elsevier Science Publishers, Amsterdam, The Netherlands, 1973.
- [2] Z. A. B. Ahmad, *Numerical simulations of LAMB-waves in plates using a semi-analytical finite element method*. PhD-Thesis, Department of Mechanical Engineering, Otto-von-Guericke-University Magdeburg, Germany, 2011.
- [3] V. Giurgiutiu, *Structural health monitoring with piezoelectric wafer active sensors*. Academic Press, Burlington, MA, USA, 2007.

- [4] K. F. Graff, *Wave motion in elastic solids*. Clarendon Press, Oxford, UK, 1975.
- [5] B. Hennings, *Elastische Wellen in faserverstärkten Kunststoffplatten - Modellierung und Berechnung mit spektralen finiten Elementen im Zeitbereich* -. PhD-Thesis, Institute of Mechanics, Helmut-Schmidt-University/University of the Federal Armed Forces Hamburg, Germany, 2015.
- [6] R. M. Jones, *Mechanics of composite materials*. Scripta Book, Washington, 1975.
- [7] M. N. Neumann, B. Hennings, R. Lammering, Quasi-continuous mode conversion of LAMB-waves in CFRP plates due to inhomogeneity on micro and meso scale. *7th European Workshop on Structural Health Monitoring*, Nantes, France, 2014.
- [8] J. L. Rose, *Ultrasonic waves in solid media*. Cambridge University Press, Cambridge, UK, 2014.
- [9] C. Willberg, S. Koch, G. Mook, J. Pohl, U. Gabbert, Continuous mode conversion of LAMB-waves in CFRP plates. *Smart Materials and Structures*, **21**, 2012.